Symmetric arrangement of mitochondria:plasma membrane contacts between adjacent photoreceptor cells regulated by Opa1

Ingrid P. Meschede[1], Miguel C. Seabra[1,2], Clare E. Futter[1], Marcela Votruba[3,4], Michael E. Cheetham[1], Thomas Burgoyne[1]

[1] UCL institute of Ophthalmology, London, EC1V 9EL

[2] CEDOC, NOVA Universidade Nova de Lisboa, Lisbon, Portugal.

[3] School of Optometry and Vision Sciences, Cardiff University, Cardiff, UK

[4] Cardiff Eye Unit, University Hospital Wales, Cardiff, UK

Corresponding Author:

Thomas Burgoyne

Tel:+442076084020

t.burgoyne@ucl.ac.uk

Classification: Biological Sciences

Keywords: rod photoreceptors, mitochondria, contact sites

Abstract

Mitochondria are known to play an essential role in photoreceptor function and wellbeing that enables normal healthy vision. Within photoreceptors they are elongated and extend most of the length inner segment, where they supply energy for protein synthesis and the phototransduction machinery in the outer segment as well as acting as a calcium store. Here we examined the arrangement of the mitochondria within the inner segment in detail using 3D electron microscopy techniques and show they are tethered to the plasma membrane in a highly specialised arrangement. This includes mitochondria running alongside each other in neighbouring inner segments, with evidence of alignment of the cristae openings. As the pathway by which photoreceptors meet their high energy demands is not fully understood, we propose this to be a mechanism to share metabolites and assist in maintaining homeostasis across the photoreceptor cell layer. In the extracellular space between photoreceptors, Müller glial processes were identified. Due to the often close proximity to the inner segment mitochondria, they may too play a role in the inner segment mitochondrial arrangement as well as metabolite shuttling. OPA1 is an important factor in mitochondrial homeostasis, including cristae remodelling; therefore, we examined the photoreceptors of a heterozygous *Opa1* knock-out mouse model. The cristae structure in the *Opa1*$^{+/-}$ photoreceptors was not greatly affected, but there were morphological abnormalities and a reduction in mitochondria in contact with the inner segment plasma membrane. This indicates the importance of key regulators in maintaining this specialised photoreceptor mitochondrial arrangement.

Introduction

Vertebrate photoreceptors are specialised neurons that provide vision by transducing light into electrical signals. The combination of phototransduction, neurotransmitter utilization, protein synthesis and transport and repolarisation after depolarisation makes the energy consumption of photoreceptors greater than all other cell types in the body (1, 2). As a consequence, failure to fulfil their energy requirements often results in visual problems including blindness. These include a number of diseases such as Leber's Hereditary Optic Neuropathy, Dominant Optic Atrophy, Neurogenic weakness, Ataxia, and Retinitis Pigmentosa (NARP) and Leigh syndrome that lead to malformed or dysfunctional mitochondria (3, 4). Most of the mitochondria of photoreceptors are housed within the inner segment (IS) region and are typically elongated running along the long axis of the photoreceptor. Within the IS mitochondria are well situated for uptake of extracellular metabolites via channels on the IS plasma membrane and can provide the necessary energy for protein synthesis and for the phototransduction machinery of the adjoined outer segment. Furthermore, photoreceptor mitochondria have been shown to act as a calcium store (5, 6). Ca2+ regulation is crucial for signalling including phototransduction, membrane excitability, energy metabolism, cytoskeletal dynamics, and transmitter release (7–10).

Dominant optic atrophy (DOA) is an autosomal disease that affects the optic nerves, leading to reduced visual acuity and preadolescent blindness (11). The most common cause of DOA are mutations in *OPA1* that codes for a dynamin-related guanosine triphosphatase (12, 13). OPA1 is required for lipid mixing and fusion of the mitochondrial inner membranes (14). In addition to the optic nerve, *OPA1* has been shown to be expressed in the retina in the photoreceptor IS (15). The role and impact of its loss of function in photoreceptors has not been well studied.

When examining published transmission electron microscopy images of mouse photoreceptors, the tissue is usually orientated longitudinally. When viewed like this, it is difficult to determine the fine positioning of mitochondria, and how this relates to the energy and storage demands within the photoreceptor IS. In this study, we set out to examine the mitochondria arrangement in detail throughout the depth of entire photoreceptor IS, as well as the cristae architecture using 3D electron microscopy analyses. As a consequence, we discover new insight into the arrangement, and morphology of mitochondria within the IS, which includes the first description of extensive contact sites between mitochondria and the plasma membrane in mammalian cells. This sheds light on the importance and myriad of roles that mitochondria play in photoreceptors and how this can be affected in disease models, such as we observed in the heterozygous *Opa1* knockout mouse model.

Results

Mitochondria from neighbouring photoreceptor inner segments are aligned to run side-by-side

To study the 3D arrangement of mitochondria within photoreceptor IS, P20 wild-type mouse eyes were prepared for serial block face scanning electron microscopy (SBFSEM). Single images from the SBFSEM data showed the mitochondria to be positioned in close proximity to the plasma membrane throughout the entire IS (Figure 1 A). The arrangement of mitochondria varied at different depths of the IS. Throughout most of the IS, mitochondria appeared to cluster adjacent to mitochondria in neighbouring photoreceptors. Reduced clustering was observed at the tip of the IS, close to the outer segments (distal end of the IS) or the Golgi (proximal end of the IS). By modelling a portion of SBFSEM data, the mitochondria from neighbouring photoreceptors can be seen to clearly run alongside each other through most of the depth of the IS (Figure 1 B and Supplementary Figure 2). Some mitochondria were seen to be forked shaped and run alongside multiple mitochondria from neighbouring cells (as shown by mitochondria modelled in blue in Figure 1 B). The mitochondrial arrangement determined from the SBFSEM data correlated with observations made from conventional transmission electron microscopy (TEM) samples of 6 month old and P20 wild-type mice (Figure 1 C, D). Mitochondria from neighbouring photoreceptors were seen running side-by-side in longitudinal samples as well as arranged in doublets or triplets in transversely orientated samples. The same mitochondrial arrangement was observed in rod and neighbouring cone photoreceptors (Supplementary Figure 1) that were identified by the higher density of less electron dense mitochondria (16). In the extracellular space between photoreceptor IS, often positioned between the mitochondria, small circular membranous structures were observed within TEM images (white arrowheads in D, E). When examined in the SBFSEM data these were found to be projections that run up between the IS (Supplementary Figure 2).

Mitochondria are tethered to the plasma membrane and the cristae between mitochondria from neighbouring cells appear to be aligned

By examining the IS mitochondria at high magnification within electron microscopy images, electron dense tethers were detected between the mitochondrial outer membrane and the plasma membrane (Figure 2 A). In addition, a high degree of consistency was found when

measuring the distance between the two membranes (Figure 2 B), which was found to be 10.77 nm (±0.28). To examine the tethering and mitochondria structure in 3D at a higher resolution than is achievable by SBFSEM, tomograms were generated (Figure 2 C). Within the tomographic data the tethers were resolved and could be seen bridging the outer mitochondrial and plasma membranes (Figure 2 D and Supplementary Video 1, 2). When examining the mitochondria cristae, at different depths within the tomograms, the opening of the cristae appeared to be aligned (77.84% ± 2.20% SD measured from 5 tomograms) between neighbouring mitochondria (Figure 2 E). This was further confirmed by modelling the mitochondria membranes indicating many of the cristae openings are opposed to each other (black dotted line in Figure 2 F & Supplementary Video 1-3).

Neighbouring cell mitochondria cristae alignment was not observed within the retinal pigment epithelium

To investigate if the alignment of the cristae across mitochondria of neighbouring cells is a general phenomenon in the retina, the retinal pigment epithelium (RPE) was examined. At the RPE lateral membrane, mitochondria are closely associated to the plasma membrane (Figure 3 A, distance between mitochondrial outer membrane and plasma membrane measured as 10.45nm ± 0.53nm SE), similar to what we observed in the photoreceptor IS. Most of these were not found to be positioned adjacent to mitochondria of neighbouring cells (42.01% ± 5.25% SE) the ones that were had little or no cristae alignment (Figure 3 B). This was in contrast to the photoreceptor IS cristae that were found to be aligned in both longitudinally and transversely orientated tissue samples (Figure 3 C, D).

Müller Glial processes run between photoreceptor outer segments

The small circular membrane observed in transversely orientated mouse retina (Fig 4 A) were seen as tubular projections running between photoreceptor IS when viewed in longitudinally orientated samples (Figure 4 B). Images from SBFSEM data showed these originated at the border between the outer nuclear and the IS layers and run up to approximately half the length of the IS (Supplementary Figure 2 and 3 A). When performing immunoEM labelling against actin (anti-β-actin in Figure 4 C and phalloidin staining in Supplementary Figure 3 B), the staining was enriched within these projections as well as at membrane junctions at the proximal IS (white and black arrowheads respectively in Figure 4 C and Supplementary Figure 3 B). This was in contrast to the IS, where no cortical actin

staining was detected at the lateral borders. A tomogram resolved the filamentous content running through the projection (Figure 4 D), likely to be actin filaments. Labelling F-actin with phalloidin highlights the actin enriched projections within the IS layer and when tilting the 3D confocal data, a 'honeycomb' like pattern was observed reflecting the membrane junctions at the proximal IS (Fig 4 E, Supplementary Figure 3 C and black arrow heads in Figure 4 A-D). To determine the origin of the projections, an antibody against glutamine synthetase was used as it is a well-known Müller glial cell marker. By immunofluorescence there was no observed colocalization other than an overlapping region of enrich staining at the base of the projections (phalloidin staining) and within the glutamine synthetase channel (Figure 4 F small panels). To investigate this further immunoEM labelling against glutamine synthetase was performed on retinal sections. This clearly showed that the projections emanated from the labelled Müller glial cells (Figure 4 G and further staining in Supplementary Figure 3 D). In agreement with the IF staining the glutamine synthetase was absent from the projections in the immunoEM labelled sections, and only present within the cell body. By highlighting the projections within the SBFSEM data they could be traced to the cells that surrounded the photoreceptor rather than the photoreceptors themselves (Figure 4 H), providing further evidence they are Müller glial cell derived.

Mitochondria arrange against the inner segment plasma membrane between postnatal day 10 and 13.

To determine the stage at which neighbouring photoreceptor IS mitochondrial align we examined mouse eyes pre- and post- full differentiation of the outer retina (before and after postnatal day 13 respectively) (17). At postnatal day 7 (P7) the immature photoreceptors (identified in the central retina by the presence of immature outer segments, highlighted by OS in Figure 5A) have a short IS consisting of scattered mitochondria, some in contact with the plasma membrane, as well as others positioned away from the plasma membrane (Figure 5 A). At P7 we observed the presence of Müller glial processes, but there was no obvious alignment between mitochondria of neighbouring IS. By P10 a greater number of mitochondria were observed positioned against the plasma membrane with some still position centrally within the IS (Figure 5 B). At this age some alignment between neighbouring IS mitochondria was observed. By P13 the mitochondrial positioning and alignment with neighbouring cell mitochondria reflected that of mature retina at P42 (Figure 5 C, D white arrowheads).

Heterozygous knockout of Opa1 alters mitochondrial positing but does not affect cristae alignment

As OPA1 is known to play a role in mitochondrial fusion and cristae morphology (18, 19) and specific deficits in visual electrophysiology (20), we examined the eyes of heterozygous knockout mice by electron microscopy. From longitudinally orientated retinal samples, the IS mitochondria of *Opa1* $^{+/-}$ mice presented an abnormal morphology and reduced alignment to neighbouring IS mitochondria when compared to *Opa1* $^{+/+}$ (Figure 6A). Retinal cross sections at different depths of the IS showed some mitochondria in the *Opa1* $^{+/-}$ mice to be larger or abnormally shaped compared to those from *Opa1* $^{+/+}$ mice (Figure 6B). The positioning of mitochondria within the IS and the mitochondrial diameter were quantified from photoreceptor cross-sections (Figure 6 C-F). The percentage of IS containing mitochondria positioned away from the plasma membrane was higher in the *Opa1* $^{+/-}$ (38.32% ± 2.31% SE) compared to the *Opa1* $^{+/+}$ (13.25% ± 4.22% SE) mouse eyes (Figure 6 C, E). Measurements of the shortest mitochondrial diameter indicated that the *Opa1* $^{+/-}$ mouse IS had larger mitochondria compared to the *Opa1* $^{+/+}$ mice (Figure 6 D, F and Supplementary Figure 4 A). Tomographic reconstructions were generated to examine the mitochondrial cristae (Figure 6 G). Within the tomographic slices, cristae openings were found to be aligned in mitochondria positioned against the plasma membrane in both the *Opa1* $^{+/-}$ and *Opa1* $^{+/+}$ IS (Figure 6 G left-hand and central panel, as well Supplementary Figure 4 B). Large mitochondria positioned away from the plasma membrane in the *Opa1* $^{+/-}$ IS did not appear to have unusual or disordered cristae (Supplementary Figure 4 B).

Discussion

The high energy demands and importance of mitochondria for calcium storage in photoreceptor required for healthy vision are well established (1, 10). Yet the arrangement of mitochondria within photoreceptor IS has not been well studied. This has largely been hampered due to the lack of techniques to image through entire IS at the resolution that is achievable by electron microscopy. The development of SBFSEM methodology allows serial imaging through large tissue volumes and is ideal for examining photoreceptor mitochondria. This combined with a range of transmission electron techniques has allowed us to make a number of important and novel findings in regard to the highly specialised mitochondrial arrangement in the IS, shedding light on how this may help regulate energy and metabolite homeostasis across the mouse photoreceptor cell layer.

When examining through the depth of mouse photoreceptor IS, mitochondria remain in contact with the plasma membrane, and were seen to cluster together in pairs or triplets. The clustered mitochondria were found to be aligned to each other, running alongside most of the length of the IS, resulting in large mitochondrial surface areas facing each other. The distance between the mitochondria outer membrane and the plasma membrane was highly consistent, and we discovered this to be maintained by tethering between the membranes. This is the first time this kind of tethering has been shown in mammalian cells, which reflects the mitochondria–plasma membrane contact sites that have been studied in yeast (21). It has been suggested from previous studies that mitochondria are tethered to the plasma membrane in mammalian brain synapses (22). As these filamentous connections have been described as cytoskeletal anchors and run between mitochondria and adhering junctions over a distance greater than that of a contact site (>30 nm), they may not be linked directly to the plasma membrane and are a different type of tethering complex than the ~11nm tether we have observed here (23–25). As there is no known mammalian homolog of the yeast mitochondria–plasma membrane tethering components Num1 and Mdm36, as well as a lack of a reliable *in vitro* photoreceptor model with fully differentiated outer segments, we were unable to determine the constituents of the IS plasma tethers (21, 22). The close association of the mitochondria to the plasma membrane and the alignment to mitochondria from neighbouring photoreceptors implies there is communication and/or sharing of resources. Photoreceptors are highly sensitive to hypoxia and nutrient deprivation, but the pathway by which they can maintain the metabolite levels to meet their high energy demands is not fully understood (26). Furthermore, studies examining metabolic flux in the retina indicate the need for energy homeostasis across the photoreceptor cell layer and with the RPE to maintain retinal health and visual acuity (27–30). Therefore, the mitochondria arrangement described in this study may be an important evolutionary development for sharing the level of particular metabolites across the photoreceptor cell layer. It is possible the position of the mitochondria at the plasma membrane assists in directing light as there is evidence nocturnal mammals have a nuclear architecture consisting of heterochromatin localised in the centre that directs light up through the inner segment to the outer segment (31). Further work is required to test these hypotheses, using techniques to measure levels of metabolites as well as energy metabolism from photoreceptor cells in different mammalian models that have a clear mitochondrial disarrangement phenotype or disrupted mitochondrial tethering to the plasma membrane.

Tomographic reconstructions of IS mitochondria were used to resolve the fine cristae architecture. Single slices from the data as well as segmentation models showed the cristae opening showed a high degree of alignment between mitochondria of neighbouring cells. To

determine if these were coincidental or exist in other cells types, RPE mitochondria were inspected. Mitochondria at the lateral RPE cell border were found to be in contact with the plasma membrane similar to what we found in IS, but most mitochondria from neighbouring cells were not found to be position side-by-side. Due to the conserved distance, we predict that there are tethers to the RPE lateral cell border, but in this study we were unable to clearly detect if they were present. When examining the cristae from the few neighbouring RPE cell mitochondria that were observed, the cristae showed little, if any, alignment when compared to what was observed in the IS. The alignment of the cristae opening further supports the notion of a mechanism for communication and/or regulate exchange of resources across plasma membranes to mitochondria of neighbouring cells. Mitochondria within mouse cardiomyocytes and human skeletal muscle have been shown to form dense inter-mitochondrial junctions that have alignment/coordination of the cristae (32, 33). This is the first time cristae alignment has been observed between mitochondria from neighbouring cells. It is possible in photoreceptors that the mitochondria are polarised so that the cristae face the plasma membrane and the cristae opening are separated evenly, which gives the appearance of alignment. The tomography slices and model indicate this is unlikely, however, as the openings do not appear to be evenly distributed and a have a similar pattern of openings when compared to the opposing mitochondrial inner membranes. Furthermore, the shape of the cristae in some of the electron microscopy images demonstrate it curving into position for alignment to a neighbouring mitochondrion. For the cristae to align across cells would require a coordinated complex at contact sites where there are cristae opening are positioned. It is known at the cristae opening there is coordination and contacts between the inner and outer mitochondria membrane leading to the positioning of particular channels (34–36). At these sites on the outer mitochondrial membrane there would likely need to be further connections bridging to the plasma membrane, where there is another process that coordinates corresponding tethers within the neighbouring cells. For this to occur it is expected there would be either; (i) further tethers between cells similar to what we observed in tomography slices, (ii) stimulation by released of metabolites/protein through plasma membrane channels or (iii) plasma membrane lipid enriched domains that are coordinated by the mitochondria to be positioned to line-up with cristae openings.

In the extracellular spaces between photoreceptors, often positioned close to the IS mitochondria, tube like projections were observed. In previously studies these have been proposed to be Müller glial processes, but there has been a lack of definitive evidence at the resolution of TEM to prove this to be the case (37, 38). To better characterise as well as determine the origin of these projections we used a combination of immuno-labelling and 3D electron microscopy techniques. We found that they were actin enriched, when staining for

actin by immuno-EM, and while doing so we did not detect cortical actin at the lateral border of the photoreceptor IS. The latter finding correlates well with our mitochondria observations within the IS, as actin filaments would likely hinder the positioning and tethering of mitochondria to the plasma membrane. By staining for glutamine synthetase a well-known Müller glial cell marker, it was found to be absent from the projections, but labelled the cells that the projections emanated from. In addition to examining images through the depth of the retina close to the IS-ONL junction by SBFSEM, the projections do not originate from photoreceptors and we unequivocally show they are Müller glial cell derived. It has been proposed in retina there is an metabolic ecosystem, and in addition to the well-established metabolic transport between the RPE and photoreceptors (39–42), Müller glial cells are involved in shuttling of lactate as well as other metabolites (27, 43, 44). Due to the positioning of the Müller glial processes close to the IS mitochondria, they may exist to assist in transport of resources towards or away from the IS mitochondria. The actin filaments within the processes likely exists to support and stabilise the structure and other systems are involved in the transport of resources.

To determine the timepoint at which the mitochondria within the IS arrange against the plasma membrane aligning to neighbouring cell mitochondria, mouse eyes with developing photoreceptors were examined. At the youngest timepoint P7, the mitochondria appeared dispersed and gradually rearranged by P13, were the mitochondria where positioned in a similar arrangement to fully developed retina at P42. The outer limiting membrane layer that forms close to the proximal inner segment will have formed by P7, as Müller glial processes were observed, indicating their presence is independent to the mitochondrial rearrangement.

To determine the effect of reducing a known regulator of mitochondrial structure, Opa1, heterozygous *Opa1* KO mouse photoreceptors were examined. In the IS there was evidence of a fusion defect in some of mitochondria, but more strikingly the mitochondria were larger, and a greater proportion were position away from the plasma membrane in the *Opa1* $^{+/-}$ compared to the *Opa1* $^{+/+}$ mice. The cristae morphology and openings were found to be unaffected, and were aligned between neighbouring cell mitochondria in the *Opa1* $^{+/-}$ mice when examined in tomographic slices. Opa1 is most highly expressed in the retina and as heterozygous KO, the expression levels may have been adequate to provide normal cristae morphology, in combination with other factors that are regulating the cristae opening alignment (45). Due to the reduced proportion of mitochondria in contact with the plasma membrane, it makes the *Opa1* $^{+/-}$ a good model for future studies to determine the pathway that leads to the specialised IS mitochondrial arrangement.

This study sheds light on the importance on mitochondria in the IS and how their position and morphology have likely evolved to help fulfil the energy and storage demands across the photoreceptor cell layer. Further work is required to identify the tethers between the mitochondria and the plasma membrane as well as the factors regulating the cristae alignment. Furthermore, the positioning of mitochondrial and tether to the plasma membrane are likely to important in other cells types.

Material and Methods

Mouse eyes

The mouse eyes used were from mice that had been sacrificed by cervical dislocation in accordance with Home Office guidance rules under project licence 70/8101 and 30/3268 This was undertaken in accordance with Animals (Scientific Procedures) Act 1986 (United Kingdom) and Home Office (United Kingdom) guidance rules, adhering to the Association for Research in Vision and Ophthalmology Statement for the Use of Animals in Ophthalmic and Vision Research. Heterozygous Opa1 KO mice were generate as previously described (46).

Transmission electron microscopy and tomography

Mouse eyes were fixed and embedded as described (47). ~100nm thick sections were cut and stained using lead citrate before acquiring images on a JEOL 1400+ TEM equipped with a Gatan Orius SC1000B charge-coupled device camera. For tomography 10-nm gold particle solution (fiducial marker) was used to stain the sections before tilting the stage from ±60° in 1.5° increments using the SerialEM software (48). The images were processed and tomograms generated using the IMOD tomography package (49).

3view serial block face scanning electron microscopy

Eyes were fixed in 3% (vol/vol) glutaraldehyde and 1% (wt/vol) paraformaldehyde in 0.08 M sodium cacodylate buffer, pH 7.4 for 2 hrs at room temperature before incubating in the following solutions; 1% aqueous osmium tetroxide and 1.5% potassium ferrocyanide at 4°C for 1 hours, 1% aqueous thiocarbohydrazide at room temperature for 20 mins and 2% aqueous osmium tetroxide at room temperature for 30 minutes. They were sequentially en bloc stained 1% (wt/vol) aqueous uranyl acetate at 4°C overnight followed by Walton's lead

aspartate 30 mins at 60°C (50). The samples were dehydrated in an ethanol series followed by propylene oxide and infiltration in a mixture of propylene oxide and Durcupan ACM resin (1:1), before embedding in Durcupan ACM resin at 60° overnight. Blocks cut from the embedded specimens were mounted onto aluminum pins and coated with gold palladium. Using a Gatan 3View system (Gatan Inc, Abingdon, UK) and a Zeiss Sigma VP field emission scanning electron microscope (Zeiss, Cambridge, UK), images were acquired in between the sequential cutting away of 100nm thick section of the sample. The images were re-aligned using the StackReg plugin (EPFL) in ImageJ (NIH) and the images were modelled using the IMOD tomography package (49).

Cryo-immuno-electron microscopy

Mouse eyes were fixed in 4% (wt/vol) paraformaldehyde and 0.1% glutaraldehyde in 0.1 M phosphate buffer at pH 7.4 for 2hrs. The cornea and were lens removed before cutting the eye cup into small blocks and embedding them in 12% (wt/vol) gelatin, followed by infusion with 2.3 M sucrose solution t at 4 °C overnigh. 80nm sections were cut at −120 °C and collected in 1:1 mixture of 2.3 M sucrose/2% (wt/vol) methylcellulose, and labeling was performed as described previously (51). Labelling of actin was performed using an anti-β-actin antibody (Sigma) or phalloidin bound to biotin (Molecular Probes) and anti-biotin (Rockland), followed by protein-A-gold (CMC, University Medical Center Utrecht).

Immunofluorescence

The eyes were fixed in 4% (wt/vol) paraformaldehyde in PBS for 2 hrs before infusing with 30% (wt/vol) sucrose at 4°C before embedding in OCT compound and freezing using a bath of acetone cooled to -78°C. 5–20 um sections of the frozen samples were cut at -20°C using a cryostat. The sections were permeabilised using 0.1% (vol/vol) saponin in PBS for 30 mins at room temperature being antibody labelling in blocking solution consisting 0.01% (vol/vol) saponin in 1% (wt/vol) BSA in PBS for 2 hrs at room temperature. The sections were incubated in the following primary antibodies; glutamine synthetase (Novus Biologicals) and RETP1 (Abcam). Secondary antibodies bound to an Alexa Fluor dye (ThermoFisher Scientific) were applied to the sections for 1 hr at room temperature before mounting mounted with ProLong Gold antifade reagent (Life Technologies) that contained DAPI to counterstain the nuclei.

Immuno-electron microscopy of cryostat sections

Mouse eyes were prepared following the methods described here (52). In brief cryostat sections were permeabilised using 0.05% (vol/vol) triton in PBS for 30 mins at room temperature and using a blocking solution containing 1% (wt/vol) BSA and 0.1% acetylated BSA in PBS, antibody labelling was performed using anti-glutamine synthetase (Novus Biologicals) for 2 hrs at room temperature. A secondary anti-rabbit bound to nano-gold (Nanoprobes) was applied in blocking solution for 2 hrs at room temperature before fixing the sections in 2% (vol/vol) glutaraldehyde, 2% (wt/vol) paraformaldehyde in 0.15 M sodium cacodylate buffer, pH 7.4 for 1 hr at room temperature. A gold enhance solution prepared in accordance with manufacturers specifications (Nanoprobes) and applied to the sections at 4°C for 10 mins. The sections were incubated in 1% (wt/vol) osmium tetroxide/1.5% (wt/vol) potassium ferrocyanide in distilled water for 1 hr at 4°C, before dehydrating in an ethanol series and embedding in epon at 60°C overnight. ~100nm thick sections were cut and images acquired on a JEOL 1400+ TEM with a Gatan Orius SC1000B charge-coupled device camera.

Acknowledgements

We would like to thank Peter Munro for his help preparing the SBFSEM samples, Camilla Pilotti, Athina Dritsoula, Dimitrios Stampoulis and David Parfitt for providing wild-type mouse eye tissue and Astrid Limb for the glutamine synthetase antibody. This work was funded by grants from the Wellcome Trust (093445 to C.E.F and 205041 to M.E.C), Fight for Sight (1936UCL to M.C.S) and the Medical Research Council (G108523 and G0700949 to M.V).

References

1. Kam JH, Jeffery G (2015) To unite or divide: mitochondrial dynamics in the murine outer retina that preceded age related photoreceptor loss. *Oncotarget* 6(29):26690–26701.

2. Wong-Riley M (2010) Energy metabolism of the visual system. *Eye Brain* 2:99–116.

3. Al-Enezi M, Al-Saleh H, Nasser M (2008) Mitochondrial Disorders with Significant Ophthalmic Manifestations. *Middle East Afr J Ophthalmol* 15(2):81–86.

4. Schrier SA, Falk MJ (2011) Mitochondrial Disorders and The Eye. *Curr Opin Ophthalmol* 22(5):325–331.

5. Giarmarco MM, Cleghorn WM, Sloat SR, Hurley JB, Brockerhoff SE (2017) Mitochondria Maintain Distinct Ca2+ Pools in Cone Photoreceptors. *J Neurosci* 37(8):2061–2072.

6. Križaj D (2012) Calcium Stores in Vertebrate Photoreceptors. *Adv Exp Med Biol* 740:873–889.

7. Fain GL, Matthews HR, Cornwall MC, Koutalos Y (2001) Adaptation in vertebrate photoreceptors. *Physiol Rev* 81(1):117–151.

8. Heidelberger R, Thoreson WB, Witkovsky P (2005) Synaptic transmission at retinal ribbon synapses. *Prog Retin Eye Res* 24(6):682–720.

9. Krizaj D, Copenhagen DR (2002) Calcium regulation in photoreceptors. *Front Biosci J Virtual Libr* 7:d2023-2044.

10. Szikra T, Križaj D (2007) Intracellular organelles and calcium homeostasis in rods and cones. *Vis Neurosci* 24(5):733–743.

11. Hudson G, et al. (2008) Mutation of OPA1 causes dominant optic atrophy with external ophthalmoplegia, ataxia, deafness and multiple mitochondrial DNA deletions: a novel disorder of mtDNA maintenance. *Brain* 131(2):329–337.

12. Alexander C, et al. (2000) OPA1 , encoding a dynamin-related GTPase, is mutated in autosomal dominant optic atrophy linked to chromosome 3q28. *Nat Genet* 26(2):211.

13. Delettre C, et al. (2000) Nuclear gene OPA1 , encoding a mitochondrial dynamin-related protein, is mutated in dominant optic atrophy. *Nat Genet* 26(2):207.

14. Meeusen S, et al. (2006) Mitochondrial Inner-Membrane Fusion and Crista Maintenance Requires the Dynamin-Related GTPase Mgm1. *Cell* 127(2):383–395.

15. Wang A-G, Fann M-J, Yu H-Y, Yen M-Y (2006) OPA1 expression in the human retina and optic nerve. *Exp Eye Res* 83(5):1171–1178.

16. Stone J, van Driel D, Valter K, Rees S, Provis J (2008) The locations of mitochondria in mammalian photoreceptors: Relation to retinal vasculature. *Brain Res* 1189:58–69.

17. Sharma RK, O'Leary TE, Fields CM, Johnson DA (2003) Development of the outer retina in the mouse. *Dev Brain Res* 145(1):93–105.

18. Cipolat S, et al. (2006) Mitochondrial Rhomboid PARL Regulates Cytochrome c Release during Apoptosis via OPA1-Dependent Cristae Remodeling. *Cell* 126(1):163–175.

19. Frezza C, et al. (2006) OPA1 Controls Apoptotic Cristae Remodeling Independently from Mitochondrial Fusion. *Cell* 126(1):177–189.

20. Barnard AR, et al. (2011) Specific deficits in visual electrophysiology in a mouse model of dominant optic atrophy. *Exp Eye Res* 93(5):771–777.

21. Hammermeister M, Schödel K, Westermann B (2010) Mdm36 Is a Mitochondrial Fission-promoting Protein in Saccharomyces cerevisiae. *Mol Biol Cell* 21(14):2443–2452.

22. Westermann B (2015) The mitochondria–plasma membrane contact site. *Curr Opin Cell Biol* 35:1–6.

23. Perkins GA, et al. (2010) The Micro-Architecture of Mitochondria at Active Zones: Electron Tomography Reveals Novel Anchoring Scaffolds and Cristae Structured for High-Rate Metabolism. *J Neurosci* 30(3):1015–1026.

24. Prinz WA (2014) Bridging the gap: Membrane contact sites in signaling, metabolism, and organelle dynamics. *J Cell Biol* 205(6):759–769.

25. Spirou GA, Rowland KC, Berrebi AS (1998) Ultrastructure of neurons and large synaptic terminals in the lateral nucleus of the trapezoid body of the cat. *J Comp Neurol* 398(2):257–272.

26. Du J, Linton JD, Hurley JB (2015) Chapter Four - Probing Metabolism in the Intact Retina Using Stable Isotope Tracers. *Methods in Enzymology*, Metabolic Analysis Using Stable Isotopes., ed Metallo CM (Academic Press), pp 149–170.

27. Kanow MA, et al. (2017) Biochemical adaptations of the retina and retinal pigment epithelium support a metabolic ecosystem in the vertebrate eye. *eLife* 6:e28899.

28. Kooragayala K, et al. (2015) Quantification of Oxygen Consumption in Retina Ex Vivo Demonstrates Limited Reserve Capacity of Photoreceptor Mitochondria. *Invest Ophthalmol Vis Sci* 56(13):8428–8436.

29. Parapuram SK, et al. (2010) Distinct Signature of Altered Homeostasis in Aging Rod Photoreceptors: Implications for Retinal Diseases. *PLOS ONE* 5(11):e13885.

30. Wubben TJ, et al. (2017) Photoreceptor metabolic reprogramming provides survival advantage in acute stress while causing chronic degeneration. *Sci Rep* 7. doi:10.1038/s41598-017-18098-z.

31. Solovei I, et al. (2009) Nuclear Architecture of Rod Photoreceptor Cells Adapts to Vision in Mammalian Evolution. *Cell* 137(2):356–368.

32. Picard M, et al. (2015) Trans-mitochondrial coordination of cristae at regulated membrane junctions. *Nat Commun* 6:6259.

33. Vincent AE, et al. (2016) The Spectrum of Mitochondrial Ultrastructural Defects in Mitochondrial Myopathy. *Sci Rep* 6:30610.

34. Harner M, et al. (2011) The mitochondrial contact site complex, a determinant of mitochondrial architecture. *EMBO J* 30(21):4356–4370.

35. Hoppins S, et al. (2011) A mitochondrial-focused genetic interaction map reveals a scaffold-like complex required for inner membrane organization in mitochondria. *J Cell Biol* 195(2):323–340.

36. von der Malsburg K, et al. (2011) Dual Role of Mitofilin in Mitochondrial Membrane Organization and Protein Biogenesis. *Dev Cell* 21(4):694–707.

37. Uga S, Smelser GK (1973) Comparative Study of the Fine Structure of Retinal MÜller Cells in Various Vertebrates. *Invest Ophthalmol Vis Sci* 12(6):434–448.

38. Woodford BarbaraJ, Blanks JanetC (1989) Localization of actin and tubulin in developing and adult mammalian photoreceptors. *Cell Tissue Res* 256(3). doi:10.1007/BF00225597.

39. Adijanto J, et al. (2014) The Retinal Pigment Epithelium Utilizes Fatty Acids for Ketogenesis IMPLICATIONS FOR METABOLIC COUPLING WITH THE OUTER RETINA. *J Biol Chem* 289(30):20570–20582.

40. Du J, et al. (2016) Reductive carboxylation is a major metabolic pathway in the retinal pigment epithelium. *Proc Natl Acad Sci* 113(51):14710–14715.

41. Reyes-Reveles J, et al. (2017) Phagocytosis-dependent ketogenesis in retinal pigment epithelium. *J Biol Chem* 292(19):8038–8047.

42. Senanayake P deS, et al. (2006) Glucose utilization by the retinal pigment epithelium: Evidence for rapid uptake and storage in glycogen, followed by glycogen utilization. *Exp Eye Res* 83(2):235–246.

43. Chao JR, et al. (2017) Human retinal pigment epithelial cells prefer proline as a nutrient and transport metabolic intermediates to the retinal side. *J Biol Chem* 292(31):12895–12905.

44. Rueda EM, et al. (2016) The cellular and compartmental profile of mouse retinal glycolysis, tricarboxylic acid cycle, oxidative phosphorylation, and ~P transferring kinases. *Mol Vis* 22:847–885.

45. Ham M, Han J, Osann K, Smith M, Kimonis V (2018) Meta-analysis of genotype-phenotype analysis of OPA1 mutations in autosomal dominant optic atrophy. *Mitochondrion*. doi:10.1016/j.mito.2018.07.006.

46. Davies VJ, et al. (2007) Opa1 deficiency in a mouse model of autosomal dominant optic atrophy impairs mitochondrial morphology, optic nerve structure and visual function. *Hum Mol Genet* 16(11):1307–1318.

47. Burgoyne T, et al. (2015) Rod disc renewal occurs by evagination of the ciliary plasma membrane that makes cadherin-based contacts with the inner segment. *Proc Natl Acad Sci U S A* 112(52):15922–15927.

48. Mastronarde DN (2005) Automated electron microscope tomography using robust prediction of specimen movements. *J Struct Biol* 152(1):36–51.

49. Kremer JR, Mastronarde DN, McIntosh JR (1996) Computer visualization of three-dimensional image data using IMOD. *J Struct Biol* 116(1):71–76.

50. West JB, et al. (2010) Structure–function studies of blood and air capillaries in chicken lung using 3D electron microscopy. *Respir Physiol Neurobiol* 170(2):202–209.

51. Slot JW, Geuze HJ, Gigengack S, Lienhard GE, James DE (1991) Immuno-localization of the insulin regulatable glucose transporter in brown adipose tissue of the rat. *J Cell Biol* 113(1):123–135.

52. Burgoyne T, Lane A, Laughlin WE, Cheetham ME, Futter CE (2018) Correlative light and immuno-electron microscopy of retinal tissue cryostat sections. *PloS One* 13(1):e0191048.

Figure legends

Figure 1. Mitochondria from neighbouring photoreceptors align through the depth of the inner segments with projections visible nearby in the extracellular space. (A) 3view SBFSEM images of mouse photoreceptors cross sections at the distal, mid and proximal ends of the inner segment. There is apparent alignment of mitochondria from neighbouring photoreceptors that is most prominent in the mid region as shown by the box with a solid outline. The white arrowheads indicate the appearance of projections that run in between the inner segments and are positioned close to the mitochondria. (B) Segmentation and modelling of select mitochondria and plasma membranes from three inner segment, showing the mitochondria running alongside each other (arrows in (B2) indicate the different views seen in (B3-5)). One of the mitochondria shown in blue bridges three mitochondria (in red) from a neighbouring inner segment. (C) Longitudinal transmission electron microscopy (TEM) section showing mitochondria from neighbouring inner segments running side-by-side. (D) TEM cross section showing mitochondria arranged in pairs or triplets between neighbouring photoreceptors (highlighted by the boxed region. Membrane projections were seen in between the inner segments in close proximity to the mitochondria (shown by the white arrowheads). These are shown at a higher magnification in (E) by the white arrowheads as well as alignment of neighbouring photoreceptor mitochondria indicated by the black arrowheads. Scale: (A) 1µm, (B-D) 500nm and (E) 100nm.

Figure 2. Visible tethers connect mitochondria to the inner segment plasma membrane and there is alignment of the mitochondrial cristae between neighbouring cells. (A) Tethers between the mitochondrial outer membrane and the plasma membrane are visible in a thick (200nm) TEM section as highlighted in cyan. (B) The distance between the mitochondrial outer member and plasma membrane is well conserved at 10.77nm (± 0.28 SE). (C-F) Tomography reconstructions and resulting models of inner segment mitochondria. (C) Is a single slice from a tomogram reconstruction and when focusing on the plasma membrane (D) tethers can be seen connecting the mitochondria to the plasma membrane (cyan) as well as structure detected between the two inner segments (yellow). (E) Single slices from the tomograms showing alignment of cristae openings of mitochondria from neighbouring photoreceptors. (F) A model of the mitochondria generated from a tomogram reconstruction. When removing the outer membrane from the model, there is visible alignment of the cristae openings. Scale: (A) 100nm, (C) 250nm, (D-E) 100nm, (F) top panels 250nm and lower panel 100nm.

Figure 3. The mitochondrial alignment is not observed in the RPE when compared to photoreceptor IS. (A) A the lateral retinal pigment epithelium (RPE) border mitochondria (in red) are in contact with the plasma membrane (in blue). (B) TEM image of mitochondria from neighbouring RPE cells including false coloured cristae show little alignment of the cristae openings. Whereas the cristae opening alignment is seen in (C) longitudinally orientated and (D) Transverse (sample prepared for 3view and has high contrast) TEM sections of neighbouring inner segment mitochondria. Scale: (A) 500nm, (B-C) 200nm and (D) 100nm.

Figure 4. Projections that run between the inner segments are actin rich and are Müller glial cell derived. (A) Electron microscopy images of cross sections at the proximal region of the inner segment. In the left panel projections running between the inner segments are shown by the white arrowheads. The right panel is closer to the photoreceptor cell body, where the projections are no longer visible junctions between the inner segments are seen (shown by black arrow). (B) Longitudinal images of the projections that can been seen extending up between the inner segments (indicated by the white arrows, and the black arrow shows the presence of junctions). (C) Immuno-EM labelling using an antibody against β-actin labelling indicates it is enriched within the projections (white arrowheads) and at junctions (black arrowhead). (D) A slice from a tomographic reconstruction, resolves the filamentous content of the projections, likely to be actin filaments. (E) Confocal stack of phalloidin stain retina, stains the projections and when tilting the stack (right panel) a ‘honeycomb’ pattern represents the actin enrichment at the junctions (shown by black arrowheads within the EM images). (F) Immunofluorescent antibody labelling of phalloidin and the Müller glial marker glutamine synthetase that have little localisation (G) Immuno-EM labelling for glutamine synthetase shows the projections that lack labelling extend from the labelled Müller glial cells. (H) SBFSEM images show that the projections (coloured in red in the middle panel) originate from the Müller glial cells surrounding the photoreceptors in the outer nuclear layer. Scale: (A-D) 250nm, (E-F) 5um, (G) 200nm and (H) left handed panels 2µm and right handed panels 500nm.

Figure 5. The mitochondria of neighbouring inner segments are not aligned until postnatal day 13. (A-D) Electron microscopy images of photoreceptor inner segments from mice of ages (A) P7, (B) P10, (C) P13 and (D) P42. The black arrowhead indicates the presence of Müller glial cell projections, white arrowheads alignment of neighbouring inner segment mitochondria and OS the outer segments. Scale: 500nm

Figure 6. Heterozygous knockout of *Opa1* leads to changes in the mitochondria morphology and positioning, but not the alignment of cristae openings. (A) Electron microscopy images of longitudinally orientated retina from *Opa1*+/+ and *Opa1*+/- mice. There is reduced overlap of neighbouring inner segment mitochondria and some mitochondria display abnormal morphology. (B) Cross-sectioning orientated retina examined at different regions of the inner segment indicate enlarged mitochondria (white arrowheads) and evidence of a mitochondrial fusion defect (black arrowheads). (C) Images from cross sections of photoreceptor inner segments in which mitochondria against the plasma membrane are false coloured in red and those away from the plasma membrane are in green. (D) Images showing larger mitochondria in the *Opa1*+/- mice photoreceptor outer segments, but no obvious morphological defects of the cristae. (E) An increase in the number of inner segments that have mitochondria positioned away from the plasma membrane in the *Opa1*+/- mice based on quantifying images similar to those shown in (C) (average = 3 eyes). (F) Measurements of mitochondrial show an increase in the average mitochondria diameter in the *Opa1*+/- mice (average = 300 mitochondria from 3 eyes). (G) Tomographic slices shows the presence of cristae opening alignment in the both the *Opa1*+/+ and *Opa1*+/- mice, and measurement there is no significant difference between the two mouse models (average = 3 tomograms). Scale: (A) 200nm, (B) 500nm, (C) 1µm, (D) 200nm and (G) 200nm.

Figure 1

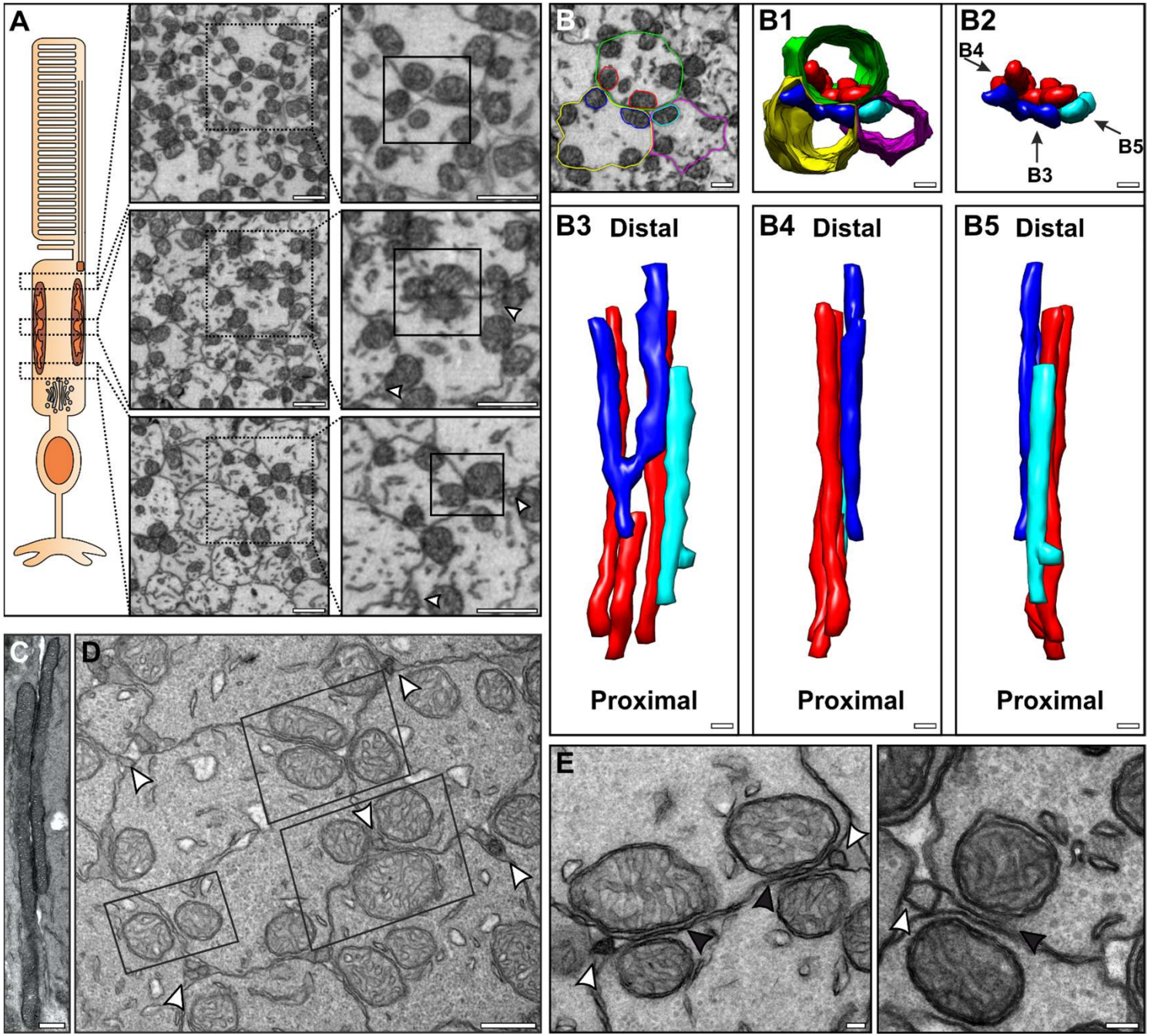
A
B
B1
B2
B4
B5
B3
B3 Distal
B4 Distal
B5 Distal
Proximal
Proximal
Proximal
C
D
E

Figure 2

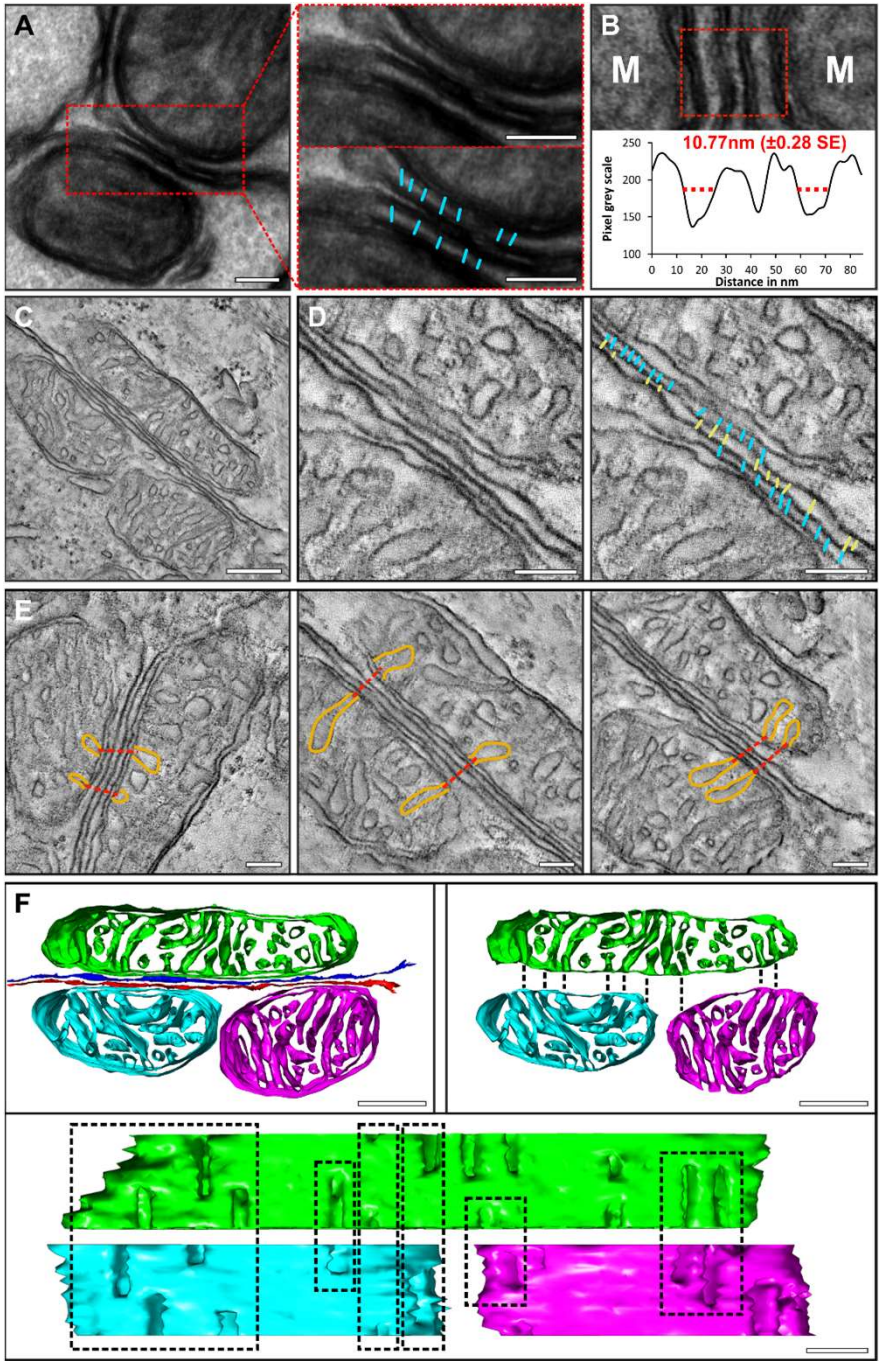
A
B
M
M
10.77nm (±0.28 SE)
Pixel grey scale
250
200
150
100
0 10 20 30 40 50 60 70 80
Distance in nm
C
D
E
F

Figure 3

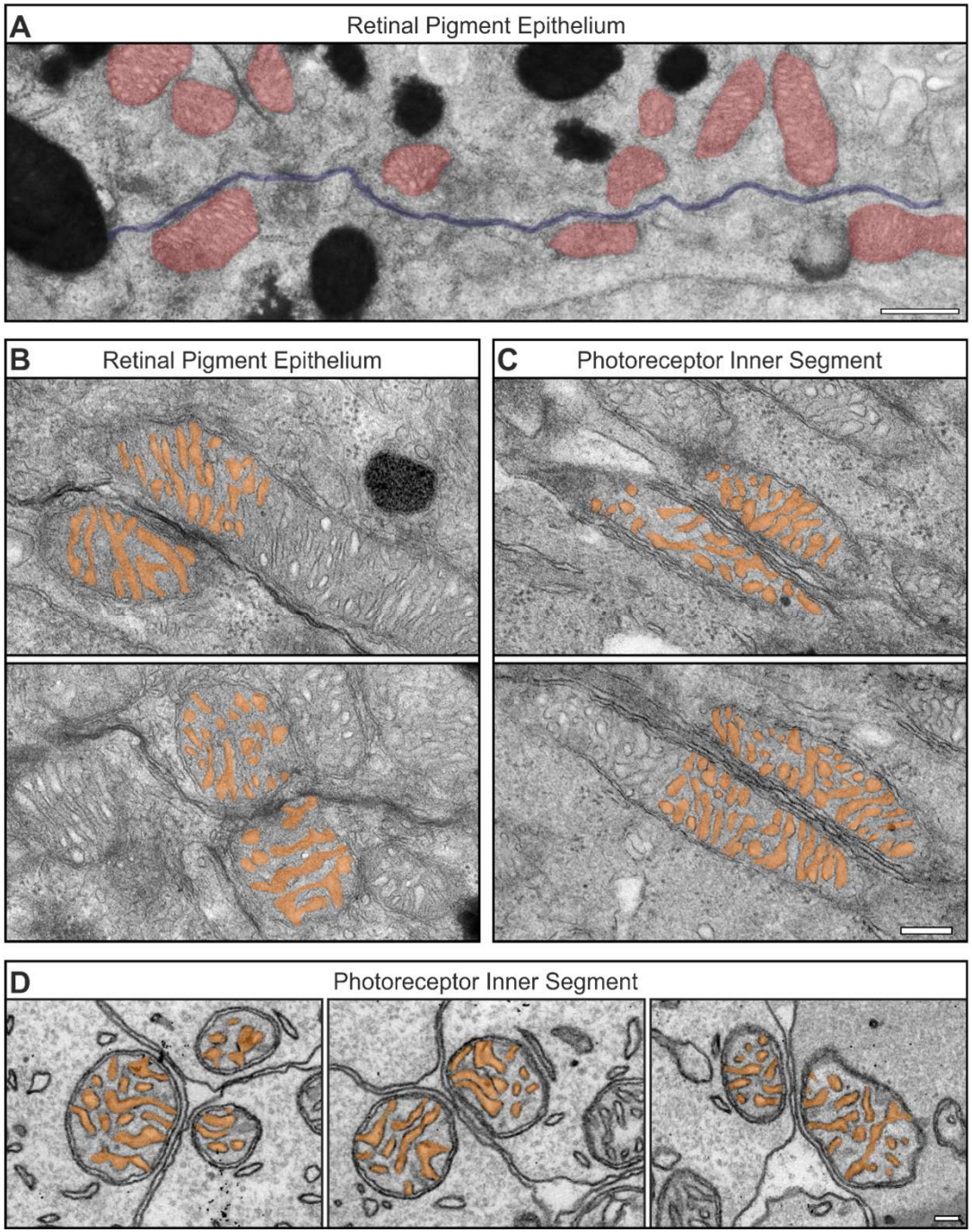
A
Retinal Pigment Epithelium
B
Retinal Pigment Epithelium
C
Photoreceptor Inner Segment
D
Photoreceptor Inner Segment

Figure 4

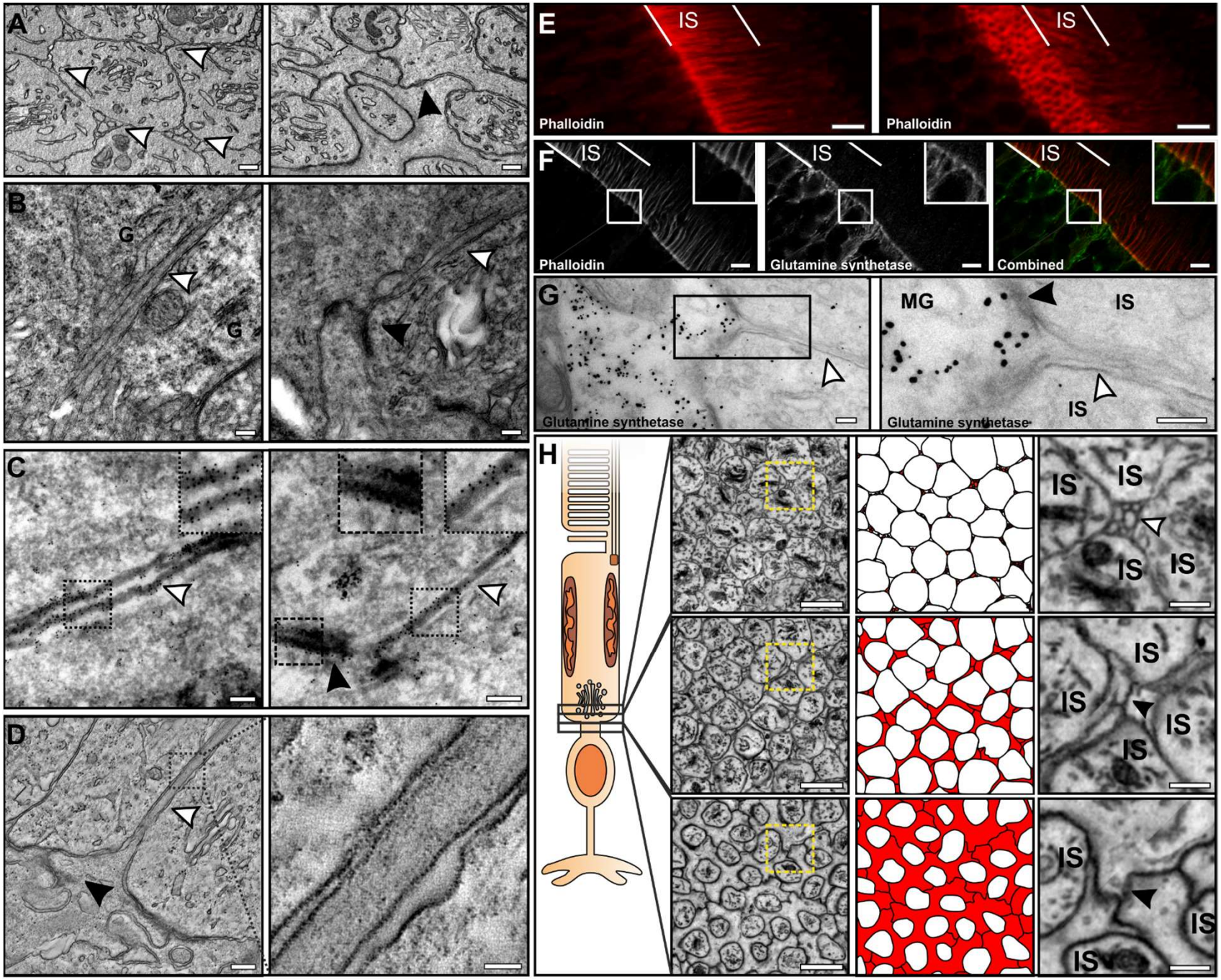
A
B
G
G
C
D
E
IS
Phalloidin
IS
Phalloidin
F
IS
Phalloidin
IS
Glutamine synthetase
IS
Combined
G
Glutamine synthetase
MG
IS
IS
Glutamine synthetase
H
IS
IS
IS
IS
IS
IS
IS
IS
IS
IS
IS
IS

Figure 5

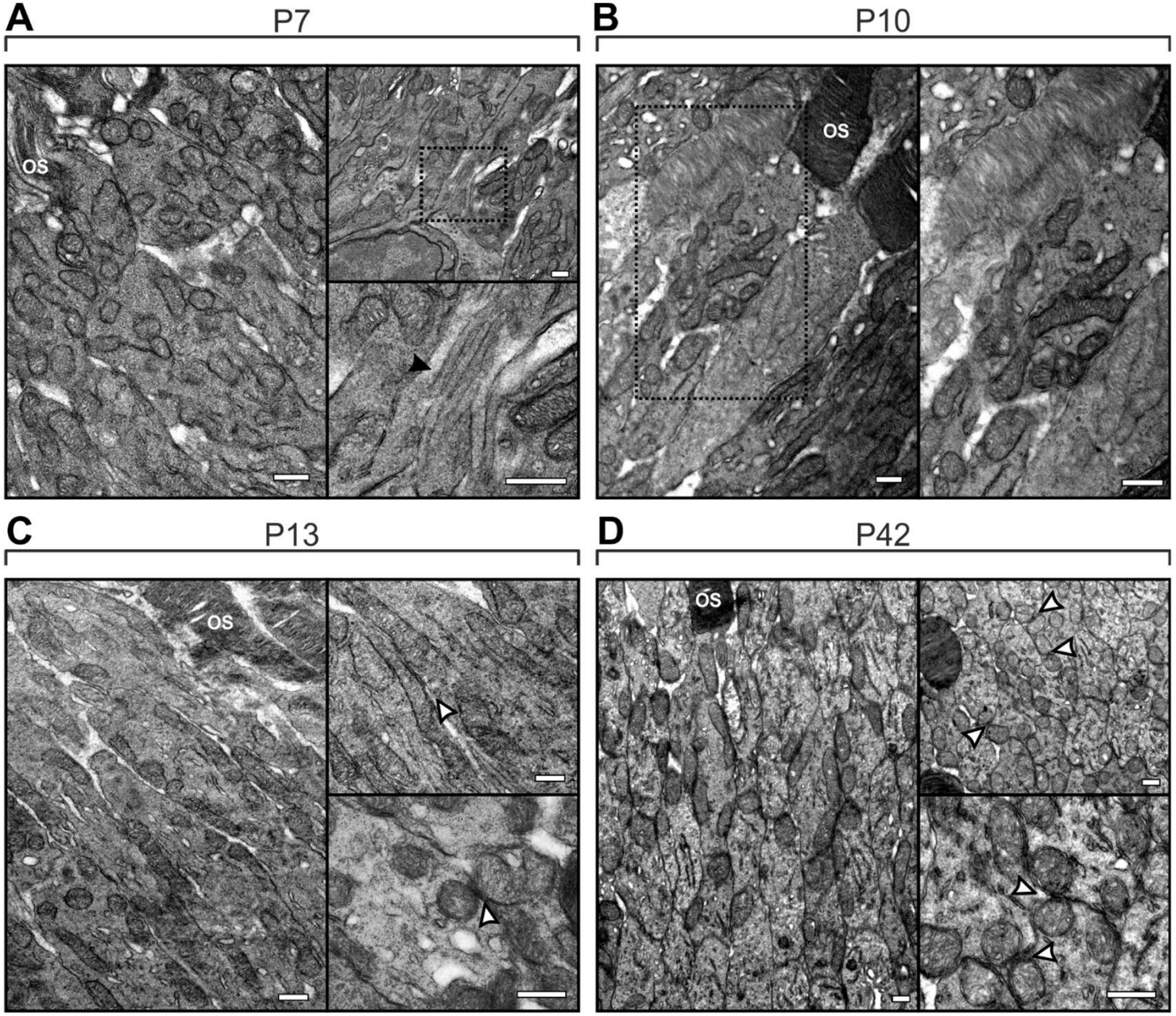

Figure 6

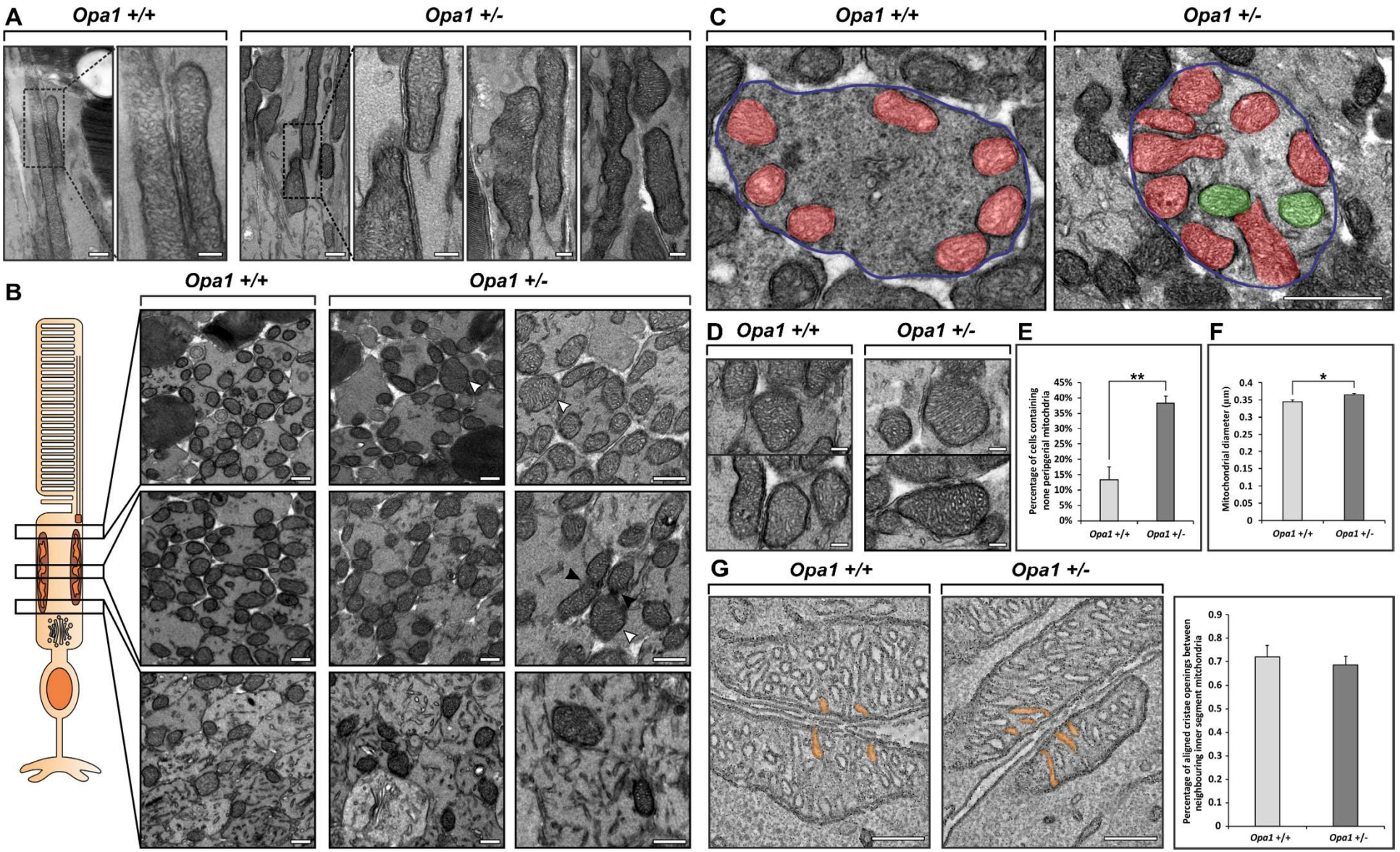
A
Opa1 +/+
Opa1 +/-
B
Opa1 +/+
Opa1 +/-
C
Opa1 +/+
Opa1 +/-
D
Opa1 +/+
Opa1 +/-
E
Percentage of cells containing none perigerial mitochdria
45%
40%
35%
30%
25%
20%
15%
10%
5%
0%
**
Opa1 +/+
Opa1 +/-
F
Mitochondrial diameter (µm)
0.4
0.35
0.3
0.25
0.2
0.15
0.1
0.05
0
*
Opa1 +/+
Opa1 +/-
G
Opa1 +/+
Opa1 +/-
Percentage of aligned cristae openings between neighbouring inner segment mitchondria
0.9
0.8
0.7
0.6
0.5
0.4
0.3
0.2
0.1
0
Opa1 +/+
Opa1 +/-